The Astrophysical Journal Letters, 820:L36 (5pp), 2016 April 1 doi:10.3847/2041-8205/820/2/L36

INTEGRAL UPPER LIMITS ON GAMMA-RAY EMISSION ASSOCIATED WITH THE GRAVITATIONAL WAVE EVENT GW150914

V. Savchenko[1], C. Ferrigno[2], S. Mereghetti[3], L. Natalucci[4], A. Bazzano[4], E. Bozzo[2], S. Brandt[5], T. J.-L. Courvoisier[2], R. Diehl[6], L. Hanlon[7], A. von Kienlin[6], E. Kuulkers[8], P. Laurent[9,10], F. Lebrun[9], J. P. Roques[11], P. Ubertini[4], and G. Weidenspointner[6,12]

[1] François Arago Centre, APC, Université Paris Diderot, CNRS/IN2P3, CEA/Irfu, Observatoire de Paris, Sorbonne Paris Cité, 10 rue Alice Domon et Léonie Duquet, F-75205 Paris Cedex 13, France
[2] ISDC, Department of astronomy, University of Geneva, chemin d'Écogia, 16 CH-1290 Versoix, Switzerland
[3] INAF, IASF-Milano, via E.Bassini 15, I-20133 Milano, Italy
[4] INAF-Institute for Space Astrophysics and Planetology, Via Fosso del Cavaliere 100, I-00133-Rome, Italy
[5] DTU Space—National Space Institute Elektrovej—Building 327 DK-2800 Kongens Lyngby, Denmark
[6] Max-Planck-Institut für Extraterrestrische Physik, Garching, Germany
[7] Space Science Group, School of Physics, University College Dublin, Belfield, Dublin 4, Ireland
[8] European Space Astronomy Centre (ESA/ESAC), Science Operations Department E-28691, Villanueva de la Cañada, Madrid, Spain
[9] APC, AstroParticule et Cosmologie, Université Paris Diderot, CNRS/IN2P3, CEA/Irfu, Observatoire de Paris, Sorbonne Paris Cité, 10 rue Alice Domont et Léonie Duquet, F-75205 Paris Cedex 13, France
[10] DSM/Irfu/Service d'Astrophysique, Bat. 709 Orme des Merisiers CEA Saclay, F-91191 Gif-sur-Yvette Cedex, France
[11] Université Toulouse; UPS-OMP; CNRS; IRAP; 9 Av. Roche, BP 44346, F-31028 Toulouse, France
[12] European XFEL GmbH, Albert-Einstein-Ring 19, D-22761, Hamburg, Germany
Received 2016 February 12; accepted 2016 March 6; published 2016 March 30

ABSTRACT

Using observations of the *INTErnational Gamma-Ray Astrophysics Laboratory* (*INTEGRAL*), we place upper limits on the gamma-ray and hard X-ray prompt emission associated with the gravitational wave event GW150914, which was discovered by the LIGO/Virgo Collaboration. The omnidirectional view of the *INTEGRAL*/SPI-ACS has allowed us to constrain the fraction of energy emitted in the hard X-ray electromagnetic component for the full high-probability sky region of LIGO triggers. Our upper limits on the hard X-ray fluence at the time of the event range from $F_\gamma = 2 \times 10^{-8}$ erg cm^{-2} to $F_\gamma = 10^{-6}$ erg cm^{-2} in the 75 keV–2 MeV energy range for typical spectral models. Our results constrain the ratio of the energy promptly released in gamma-rays in the direction of the observer to the gravitational wave energy $E_\gamma/E_{\rm GW} < 10^{-6}$. We discuss the implication of gamma-ray limits for the characteristics of the gravitational wave source, based on the available predictions for prompt electromagnetic emission.

Key words: gamma-ray burst: general – gravitational waves

1. INTRODUCTION

Gravitational waves were predicted nearly one hundred years ago as a natural consequence of general relativity (Einstein 1916, p. 688), but up to now only indirect evidence of their existence has been found by measuring the time evolution of orbital parameters of binary pulsars (Hulse & Taylor 1975; Kramer et al. 2006). The direct detection of gravitational waves is challenging since it relies on measurements of the relative change in distance of the order of 10^{-22}. This will be achieved, for low frequency signals (10^{-4}–1 Hz), with the space-based eLISA mission that will be launched after 2030 (Amaro-Seoane et al. 2012), and it is currently possible at higher frequency signals (10–10^4 Hz), thanks to the ground-based advanced LIGO (LIGO Scientific Collaboration et al. 2015) and Virgo (Acernese et al. 2015) detectors. Advanced LIGO has been in operation since 2015 September, with the first science run extending to 2016 January and a sensitivity-enabling routine detection of gravitational waves from merging compact binaries. Once a possible trigger has been recorded, it is vital to conduct multi-wavelength observations to search for additional information about this event. The LIGO/Virgo Collaboration recently reported the first gravitational wave event, GW150914, detected on 2015 September 14 at 09:50:45 UTC, with a false alarm probability of less than one event per 203,000 years (Abbott et al. 2016; The LIGO Scientific Collaboration & the Virgo Collaboration 2016). Here, we exploit the data obtained by the *INTErnational Gamma-Ray Astrophysics Laboratory* (*INTEGRAL*) satellite (Winkler et al. 2003), which was fully operational at the time of the gravitational wave trigger, to derive limits on the hard X-ray and gamma-ray emission associated with this event.

2. *INTEGRAL*/SPI-ACS

The SPI instrument on board *INTEGRAL* (Vedrenne et al. 2003) is comprised of an active anticoincidence shield (ACS, von Kienlin et al. 2003) made of 91 BGO (Bismuth Germanate, $Bi_4Ge_3O_{12}$) scintillator crystals.[13] Besides its main function of shielding the SPI germanium detectors, the ACS is also used as a nearly omnidirectional detector of transient events, with a large effective area (up to 1 m^2) at energies above ~75 keV (von Kienlin et al. 2003). The ACS data consist of event rates integrated over all the scintillator crystals, with a time resolution of 50 ms. The typical number of counts per 50 ms time bin ranges from about 3000 to 6000 (or more during periods of high solar activity). Since only a single integrated rate is recorded for the whole instrument, no spectral and directional information is available. Contrary to most instruments designed for the detection of GRBs, the ACS read-out does not rely on any trigger. Thus a complete time history of

[13] Only 89 are currently functional.

Table 1
3σ Upper Limit on the Possible Gamma-Ray Counterpart Fluence

Time Scale (s)	Total Counts	Fluence (erg cm^{-2})	
		Best 95%	Worst 5%
10	4319	(3.5–4.5) × 10^{-7}	(1.1–1.4) × 10^{-6}
1	1410	(1.3–1.5) × 10^{-7}	(3.7–4.7) × 10^{-7}
0.25	727	(5.8–7.6) × 10^{-8}	(1.9–2.4) × 10^{-7}
0.1	200	(1.6–2.1) × 10^{-8}	(5.2–6.6) × 10^{-8}
0.05	220	(1.8–2.3) × 10^{-8}	(5.7–7.3) × 10^{-8}

Note. The fluence range is calculated in the 75–2000 keV range, assuming two standard hard and soft GRB spectra, characterized by a smoothly broken power law (Band model; Band et al. 1993) with parameters $\alpha = -0.5$, $\beta = -1.5$, $E_{\rm peak} = 1000$ keV, and $\alpha = -1.5$, $\beta = -2.5$, $E_{\rm peak} = 500$ keV. The best sensitivity applies to 95% of the trigger localization region; for the remaining 5% we provide a less constraining limit.

the detector count rate is continuously recorded for ∼90% of the time[14] and simultaneously covers nearly the whole sky.

SPI is partially surrounded by the satellite structure and by the other *INTEGRAL* instruments, which, by shielding the incoming photons, affect the response of the ACS in different directions. Therefore, the ACS response must be determined through detailed simulations that take into account the whole satellite structure. We developed a *GEANT3* Monte-Carlo model based on the *INTEGRAL* mass model (Sturner et al. 2003) and simulated the propagation of monochromatic parallel beams of photons in the 50 keV–100 MeV range. For each energy we simulated 3072 sky positions (16-side *HEALPix*[15] grid). This enables us to generate an instrumental response function for any sky position, which can then be used to compute the expected number of counts for a given intrinsic source spectrum. We have verified that the response produces valid results for the bursts detected simultaneously by SPI-ACS and other detectors, primarily *Fermi*/GBM, with an accuracy better than 20%.

3. RESULTS

SPI-ACS was operating nominally at the time of the LIGO trigger on 2015 September 14 at 09:50:45 UTC, yielding an uninterrupted count rate from 33 hr before to 19 hr after the event. The background was relatively stable and low, with a rate of ∼7 × 10^4 counts s^{-1}. The main limit to the sensitivity is set by the Poisson noise in the background rate. In addition to the high-count rate approximation of the Poisson process, there is an excess variance that changes from 3% to 10% on a timescale of the order of one year, and increases in case of strong solar activity. This excess noise is related to multiple events in the detector and to the solar activity. The total noise at every timescale can still be described by a Gaussian process (Savchenko et al. 2012). We measure the average background and its variance in the vicinity of the region of interest, from −1000 to +1000 s from the trigger, and use it for the computation of the significance and upper limits.

We investigated the light curve at −30 to +30 s from the trigger time on 5 timescales from 0.05 to 10 s. These timescales correspond to the expected accretion timescales in the compact binary coalescence (Lee & Ramirez-Ruiz 2007). We do not detect any obvious signal that is coincident with the GW trigger. We derived a maximum post-trial peak significance of ∼0.5σ, with a timescale of 1 s, at 26.4 s after the GW trigger. Such an excess is clearly not significant.

A zoom-in on the light curve from −10 to +10 s around the trigger time is shown in Figure 1. The excess at T_0-3 s, where T_0 is the GW trigger time, is compatible with regular background variability. A similar but negative deviation can be seen at T_0+7 s.

The upper limit on the total number of observed photons depends on the assumed duration of the event. The results for different search timescales are summarized in Table 1. The dependence of the upper limit on the burst duration remains the same for any sky position or burst spectrum. In what follows we assume a typical duration for a short GRB, 1 s.

In order to put an upper limit on the signal fluence, we have to investigate the different assumptions on the spectrum and sky coordinates. Figure 2 shows the upper limit on the 75–2000 keV fluence in 1 s for a typical short hard GRB

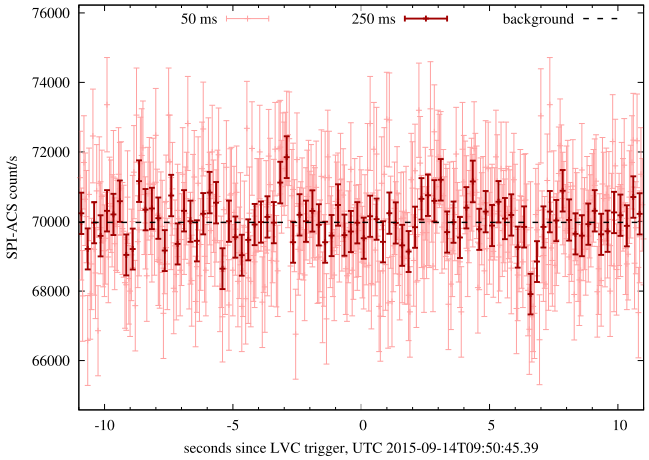

Figure 1. *INTEGRAL*/SPI-ACS light curve in ±10 s around GW150914 trigger time. Light red symbols represent the measurements at the natural instrument time resolution of 50 ms; dark red points are rebinned to 250 ms. The dashed black curve is the background level estimated from a long-term average.

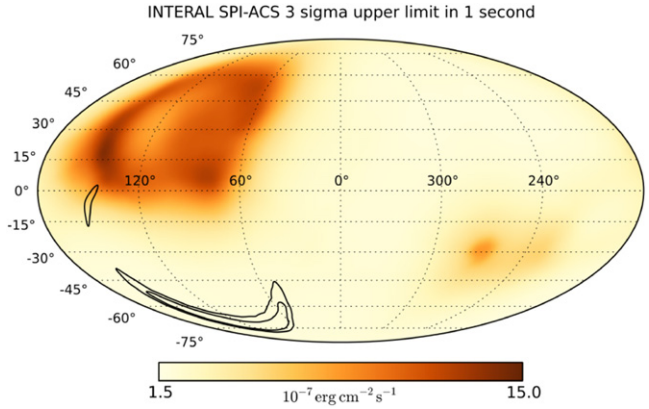

Figure 2. *INTEGRAL*/SPI-ACS 3σ upper limit in 1 s for a characteristic short hard GRB spectrum: Band model with parameters $\alpha = -0.5$, $\beta = -2.5$, $E_{\rm peak} = 1000$ keV. In the black contour regions (50% and 90%) we show the most accurate GW150914 trigger localization from the LALInference (LIGO/Virgo Scientific Collaboration 2016).

[14] Instruments are switched-off near the perigee of every revolution; until 2015 January, the *INTEGRAL* orbit lasted three sidereal days. Afterward, it was reduced to 2.7 sidereal days to allow for a safe satellite disposal in 2029.
[15] http://healpix.sourceforge.net

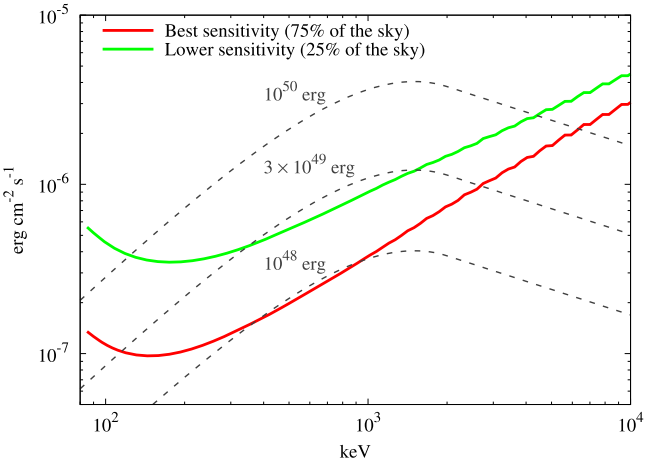

Figure 3. *INTEGRAL*/SPI-ACS 3-sigma sensitivity as a function of energy averaged over each of the two sky regions, corresponding to optimal orthogonal orientation and the least favorable directions shaded by heavy satellite material. Dashed curves correspond to the hard GRB spectrum used in Figure 2, scaled to reproduce several values of the total energy released in the 75–2000 keV band, assuming a distance to the source of 410 Mpc.

spectrum: a smoothly broken power law (Band model) with parameters $\alpha = -0.5$, $\beta = -2.5$, $E_{\rm peak} = 1000$ keV (Ghirlanda et al. 2009). SPI-ACS observed the full sky, particularly covering about 95% of the GW150914 localization confidence area, with a sensitivity that was at most 20% lower than that reached in the most favorable position. The weighted average of the limiting fluence in this region is 4% higher than that of the best, while it is a factor of 3 less favorable over the remaining 5% of the localization region. The reduced sensitivity is caused by the opacity of the satellite structure and the other *INTEGRAL* instruments. The limit depends, however, on the incident spectrum: for harder spectra the low-sensitivity regions are less pronounced. Figure 3 illustrates the energy dependency of the SPI-ACS sensitivity for two sky regions. The low-energy threshold of ACS around 75 keV limits our low-energy sensitivity. At high energy, the effective area is approximately constant, slowly increasing above 1 MeV. A spectrum typical for a hard gamma-ray burst (Band model with parameters $\alpha = -0.5$, $\beta = -2.5$, $E_{\rm peak} = 1000$ keV) is scaled to reproduce different values of the total energy release in the 75–2000 keV band, assuming a distance of 410 Mpc.

3.1. IBIS Results

The IBIS instrument (Ubertini et al. 2003) is composed of two detectors, ISGRI (20–1000 keV; Lebrun et al. 2003) and PICsIT (175 keV–10 MeV; Di Cocco et al. 2003), which, using a coded mask, provide images over a field of view of $30^\circ \times 30^\circ$. The ISGRI data are used to automatically search and localize in real time GRBs and other transients through the *INTEGRAL* Burst Alert System (IBAS; Mereghetti et al. 2003). IBAS did not reveal any new transients in the IBIS field of view at the time of the LIGO trigger, down to a peak flux sensitivity of $\sim$0.1 ph cm^{-2} s^{-1} (20–200 keV, 1 s integration time). We also carried out an offline search in the time interval 09:28–10:00 UT, again with negative results. Note, however, that the instruments of *INTEGRAL* were pointed at a position (R.A. = 271°, decl. = –31°) outside the high-probability region of the gravitational signal. This also prevented the X-ray monitor instrument JEM-X (Lund et al. 2003) from collecting constraining data.

IBIS can also provide a response to photons outside the field of view, due to high-energy photons passing through the passive and active shields of the instrument, allowing the detection of transient events. Indeed, most of the shielding of IBIS is passive and relatively thin, becoming transparent to photons above $\sim$200 keV. For high-energy events, ratemeters for the PICsIT detector are available in 8 energy bands in the range 210–2600 keV. We investigated the count rate light curve in $\pm$10 s around the GW150914 for possible excesses on timescales from 0.016 to 10 s, but found no positive signal. We set 3σ upper limits to fluences in the 570–1200 keV energy range of 2.5×10^{-7} erg cm^{-2} and 6.5×10^{-7} erg cm^{-2}, assuming durations of 1 s and 10 s, respectively. These values apply to a fully exposed detector area. The detection efficiency is highly dependent on the source position and it is considerably reduced for sources located at large angles with respect to the instrument pointing direction, due to the lower exposed area and the presence of the 2 cm-thick BGO anticoincidence shield. The localization region of GW150914 is positioned at a large offset ($\sim$80° to 140°) from the telescope axis. This implies that the sensitivity is decreased and is strongly dependent on the source position in the sky. Nevertheless, the PICsIT observation provides an important independent limit on gamma-ray emission above 500 keV associated with the GW150914.

3.2. On the Fermi/GBM Candidate

The *Fermi*/GBM team reported a possible hard X-ray transient on 2015 September 14 at 09:50:45.8 UTC, about 0.4 s after the reported LIGO burst trigger time, and lasting for about one second (Blackburn et al. 2015; Connaughton et al. 2016). The light travel time can introduce a time difference between *INTEGRAL* and *Fermi* detections of up to $\pm$0.5 s, depending on the source position within the LVC error region. We do not observe any excess within a -0.5 s to $+0.5$ s window around the *Fermi*/GBM trigger (Figure 1), and set a 3σ upper limit of 1.5×10^{-7} erg cm^{-2} for a one-second integration time, assuming a typical short hard GRB, characterized by a Band model with parameters $\alpha = -0.5$, $\beta = -2.5$, $E_{\rm peak} = 1000$ keV. A substantial part of the candidate event in the GBM comes from the high-energy BGO detector, above 100 keV (Blackburn et al. 2015), where the *Fermi*/GBM effective area is about a factor of 30–40 smaller than that of the *INTEGRAL*/SPI-ACS.

Connaughton et al. (2016) find that preferable localization of their candidate is in the direction of the Earth, or close to it, limited to the southern, dominant, arc of the GW150914 localization. Assuming the preferred localization, they conclude that the spectrum can be best fit by a hard power law with a slope of -1.4 and a 10–1000 keV fluence of $2.4^{+1.7}_{-1.0} \times 10^{-7}$ erg cm^{-2}. Extrapolating this spectrum to the full 75 keV–100 MeV energy range accessible to the SPI-ACS without a cutoff is clearly unphysical and incompatible with the SPI-ACS upper limit. However, no best-fit parameters for a model comprising a cutoff power law are reported. On the other hand, Connaughton et al. (2016) found a best fit to the Comptonized model in the northeastern tip of the the southern arc, with a power-law index $\alpha^{\rm COMP} = -0.16$ and $E^{\rm COMP}_{\rm peak} = 3500$ keV, harder than a typical *Fermi*/GBM spectrum. We assume this spectral model to compute the expected signal in the SPI-ACS: for the southern (northern) arc,

SPI-ACS would detect 4740 (1650) counts, with a signal significance of 15σ (5σ) sigma above the background. It should be noted that the northern arc is disfavored by both the GBM and the LIGO localizations.

We stress that to compare the GBM and SPI-ACS sensitivities, it is inappropriate to use a soft spectral model, as in the computation of our early fluence upper limits (Ferrigno et al. 2015), since the spectral properties of the GBM candidate are very different.

Considering the reported hardness of the GBM candidate, and the favorable orientation of the SPI-ACS with respect to the GW150914 localization, we are inclined to claim that the non-detection by SPI-ACS disfavors a cosmic origin for the *Fermi*/GBM excess. If the origin of the event was near the Earth, *INTEGRAL* would not detect it, due to the large *INTEGRAL*—Earth distance at the time of GW150914 (140,000 km). Connaughton et al. (2016) discussed a possible terrestrial origin for the GBM excess and came to the conclusion that such an origin is not compatible with the characteristics of a terrestrial gamma-ray flash. However, they do not exclude the possibility that the event had a magnetospheric origin. Eventually, considering that the false alarm probability of the GBM association is relatively high (0.2%; Connaughton et al. 2016) and that SPI-ACS does not detect it, it is likely that the GBM excess is a random background fluctuation.

4. DISCUSSION

4.1. Model-independent Limit

INTEGRAL/SPI-ACS is the only instrument covering the whole GW150914 position error region at the time of the GW trigger. The limit depends on the position, burst duration, and the assumed spectral model, and ranges from $F_\gamma = 2 \times 10^{-8}\,\mathrm{erg\,cm^{-2}}$ to $F_\gamma = 10^{-6}\,\mathrm{erg\,cm^{-2}}$ in the 75 keV–2 MeV energy range for a typical range of GRB models and sky positions (see Figure 3). Assuming a reference distance to the event of $D = 410$ Mpc (Abbott et al. 2016), this implies an upper limit on the isotropic equivalent luminosity of $E_\gamma < 2 \times 10^{48}\,\mathrm{erg}\left(\frac{F_\gamma}{10^{-7}\,\mathrm{erg\,cm^{-2}}}\right)\left(\frac{D}{410\,\mathrm{Mpc}}\right)^2$. The LIGO observation corresponds to the energy emitted in gravitational waves $E_{\mathrm{GW}} = 1.8 \pm 0.3 \times 10^{54}\,\mathrm{erg}$. Our SPI-ACS upper limit constrains the fraction of energy emitted in gamma-rays in the direction of the observer: $f_\gamma < 10^{-6}\left(\frac{F_\gamma}{10^{-7}\,\mathrm{erg\,cm^{-2}}}\right)\left(\frac{E_{\mathrm{GW}}}{1.8 \times 10^{54}\,\mathrm{erg}}\right)^{-1}\left(\frac{D}{410\,\mathrm{Mpc}}\right)^2$.

4.2. BH+BH and Circumbinary Environment

Our analysis of the gravitational wave signal indicates that it was produced by the coalescence of two black holes (Abbott et al. 2016). If at least one of the merging black holes was charged, following the Reissner–Nordstrom formulation, up to 25% of the gravitational energy could have been converted into electromagnetic radiation (Zilhão et al. 2012). However, it is expected that the charge of the black hole is spontaneously dissipated and is not significant for astrophysical applications. To date, there is no theoretical work predicting electromagnetic emission from the coalescence of two non-charged back holes in a vacuum. Indeed, it is not possible to create photons in a system with no matter outside of the gravitational horizon and only gravitational interaction involved, without invoking effects of quantum gravity, a theory which has not yet been developed.

The coalescing black holes may be surrounded by matter, in the form of spherically symmetric inflow or/and an accretion disk, which can form if the inflow possesses sufficient angular momentum. The accretion disk can have high density and large potential energy. Rapid changes in the accretion dynamics during binary coalescence may lead to bright observational signatures (Farris et al. 2012). Magnetic fields, anchored in the accretion disk, can cause bright radio emission that is simultaneous with the gravitational waves (Mösta et al. 2010).

While supermassive black holes are often accompanied by substantial disks, black holes of stellar mass lose the disk created during the progenitor star collapse on a timescale of the order of $\tau_{\mathrm{disk}} \sim 100$ s (Woosley 1993). Sustainable accretion disks can be expected when a constant inflow of matter is provided by a companion star: in these cases, the black hole—star binary can be a bright and variable X-ray and gamma-ray source. However, it remains to be established how likely it is to find a dynamically stable triple system composed of a binary black hole and an additional companion star.

Isolated stellar-mass black holes or binary black holes are bound to accrete from the interstellar medium (ISM). This process can be described as quasi-spherical Bondi–Hoyle accretion (Bondi & Hoyle 1944), characterized by very low accretion rates $\dot{M} \sim 10^{15}\,\mathrm{g\,s^{-1}}\left(\frac{M_H}{65 \times M_\odot}\right)^2\left(\frac{\rho_\infty}{10^{-24}\,\mathrm{g\,cm^{-3}}}\right)\left(\frac{c_s}{10\,\mathrm{km\,s^{-1}}}\right)^{-3}$. In the case of a merger the accretion rate may be enhanced by up to two orders of magnitude on a one-second timescale (Farris et al. 2010), but in the case of a stellar black hole binary accreting from the ISM, the isotropic peak luminosity cannot exceed $L_{\mathrm{iso}} = 100 \times 0.3 \times \dot{M}c^2 = 2.5 \times 10^{37}\ \mathrm{erg\,s^{-1}}\left(\frac{M_H}{65\,M_\odot}\right)^2\left(\frac{\rho_\infty}{10^{-24}\,\mathrm{g\,cm^{-3}}}\right)\left(\frac{c_s}{10\,\mathrm{km\,s^{-1}}}\right)^{-3}$. This luminosity is almost 17 orders of magnitude lower than the GW luminosity and more than ∼11 orders of magnitude below the current gamma-ray upper limits. Agol & Kamionkowski (2002) calculated a possible range of Bondi–Hoyle accretion rates in a Milky Way-like galaxy, yielding, in very rare cases, $\dot{M} \sim 10^{17}\,\mathrm{g\,s^{-1}}$ or peak luminosity $L_{\mathrm{iso}} = 3 \times 10^{39}\ \mathrm{erg\,s^{-1}}$, still a factor of 10^9 below what is observable. The conditions necessary to produce observable emission may be reached in dense molecular clouds, where $\left(\frac{\rho_\infty}{10^{-16}\,\mathrm{g\,cm^{-3}}}\right)\left(\frac{c_s}{1\,\mathrm{km\,s^{-1}}}\right)^{-3} > 1$. Therefore, our upper limit on the hard X-ray burst associated with the merger disfavors the possibility that the binary was embedded in such a cloud, unless the emission was very anisotropic.

Recently, different mechanisms for producing the gamma-ray emission in a black hole binary merger were suggested. For example, a binary black hole with a very small separation could be formed immediately after the collapse of a massive star, resulting in a gamma-ray burst produced nearly simultaneously with a gravitational wave signal (Loeb 2016). Alternatively, if an unusually long-lived disk is present around the black hole binary it could produce a bright gamma-ray signature at the time of the coalescence (Perna et al. 2016).

4.3. Alternative Possibilities

Abbott et al. (2016) were able to make use of the gravitational wave data to constrain the compactness of the

merging objects, excluding the possibility that either of them is a neutron star.

Strange stars are more compact than neutron stars, and their coalescences can have different gravitational wave signatures (Moraes & Miranda 2014). Very exotic equations of state for strange quark stars would allow them to reach 6 $M_{\odot}$ (Kovács et al. 2009, not considering rotation). This is well below the 90% lower limit inferred for this event (25 $M_{\odot}$).

Boson Stars (see Schunck & Mielke 2003 for a review) might reach arbitrarily high masses, while only being slightly bigger than their gravitational radius. The existence of these objects requires an extension of the minimal standard model with a new fundamental scalar field, responsible for a stable particle. The properties of this field would determine the macroscopic properties of boson stars. This field has to be compatible with the non-detection established by particle physics experiments on Earth, cosmological simulations, and models of stellar evolution. Because of these limitations, the preferred model is generally a field with minimal coupling to standard model fields. A boson star consisting of a non-charged scalar field cannot be directly involved in any electromagnetic radiation, even in the case of an energetic coalescence event. On the other hand, the coalescence of boson stars might have distinct gravitational wave signatures (Palenzuela et al. 2007).

Another exotic star type, Q-stars (Bahcall et al. 1989, 1990; Miller et al. 1998; where Q here does not stand for quark) can reach 10 or even 100 solar masses. The existence of these objects was suggested based on finding the possibility of a peculiar baryonic state of matter, without introducing new matter fields. No predictions on their coalescence exist, to the best of our knowledge.

5. CONCLUSIONS

We have derived an upper limit on the gamma-ray emission associated with the gravitational wave event GW150914 for the whole localization region with *INTEGRAL*. This sets an upper limit on the ratio of the energy directly released in gamma-rays in the direction of the observer to the gravitational wave energy $E_{\gamma}/E_{\rm GW} < 10^{-6}$ (E_{γ} in 75–2000 keV). This limit excludes the possibility that the event is associated with substantial gamma-ray radiation, directed toward the observer.

The LIGO trigger reconstruction favors a binary black hole scenario. In this case, almost no detectable gamma-ray emission is expected, unless the binary is surrounded by a very dense gas cloud, and the emission caused by the enhancement of the accretion rate during the coalescence is directed toward the observer.

If at least one of the objects is an exotic star (an unusually massive quark star, boson star, Q-star, etc.), some electromagnetic emission cannot be excluded. Unfortunately, very few predictions for electromagnetic signatures of exotic star coalescence are available so far, and our upper limit provides a constraint for future modeling.

For the first time we have set an upper limit on the gamma-ray emission associated with a binary black hole merger. This is the tightest limit that can be set on GW150914 with any modern instrument in the gamma-ray energy range. The emerging possibility of combining observations of gravitational waves and electromagnetic radiation foreshadows the beginning of a new era in multi-messenger astrophysics.

This work is based on observations with *INTEGRAL*, an ESA project with instruments and a science data center funded by ESA member states (especially the PI countries: Denmark, France, Germany, Italy, Switzerland, Spain), and with the participation of Russia and the USA. The SPI-ACS detector system has been provided by MPE Garching/Germany. We acknowledge the German *INTEGRAL* support through DLR grant 50 OG 1101. The Italian *INTEGRAL*/IBIS team acknowledges the support of ASI/INAF agreement No. 2016-025-R.0. Some of the results in this paper have been derived using the *HEALPix* (Górski et al. 2005) package. We are grateful to the François Arago Centre at APC for providing computing resources, and to VirtualData from LABEX P2IO for enabling access to the StratusLab academic cloud.

REFERENCES

Abbott, B. P., Abbott, R., Abbott, T. D., et al. 2016, PhRvL, 116, 061102
Acernese, F., Agathos, M., Agatsuma, K., et al. 2015, CQGra, 32, 024001
Agol, E., & Kamionkowski, M. 2002, MNRAS, 334, 553
Amaro-Seoane, P., Aoudia, S., Babak, S., et al. 2012, CQGra, 29, 124016
Bahcall, S., Lynn, B. W., & Selipsky, S. B. 1989, NuPhB, 325, 606
Bahcall, S., Lynn, B. W., & Selipsky, S. B. 1990, ApJ, 362, 251
Band, D., Matteson, J., Ford, L., et al. 1993, ApJ, 413, 281
Blackburn, L., Briggs, M. S., Burns, E., et al. 2015, GCN, 18339
Bondi, H., & Hoyle, F. 1944, MNRAS, 104, 273
Connaughton, V., Burns, E., Goldstein, A., et al. 2016, arXiv:1602.03920
Di Cocco, G., Caroli, E., Celesti, E., et al. 2003, A&A, 411, L189
Einstein, A. 1916, Sitzungsber K. Preuss. Akad. Wiss., 1, 688
Farris, B. D., Gold, R., Paschalidis, V., Etienne, Z. B., & Shapiro, S. L. 2012, PhRvL, 109, 221102
Farris, B. D., Liu, Y. T., & Shapiro, S. L. 2010, PhRvD, 81, 084008
Ferrigno, C., Savchenko, V., Mereghetti, S., et al. 2015, GCN, 18354
Ghirlanda, G., Nava, L., Ghisellini, G., Celotti, A., & Firmani, C. 2009, A&A, 496, 585
Górski, K. M., Hivon, E., Banday, A. J., et al. 2005, ApJ, 622, 759
Hulse, R. A., & Taylor, J. H. 1975, ApJL, 195, L51
Kovács, Z., Cheng, K. S., & Harko, T. 2009, MNRAS, 400, 1632
Kramer, M., Stairs, I. H., Manchester, R. N., et al. 2006, Sci, 314, 97
Lebrun, F., Leray, J. P., Lavocat, P., et al. 2003, A&A, 411, L141
Lee, W. H., & Ramirez-Ruiz, E. 2007, NJPh, 9, 17
LIGO Scientific Collaboration, Aasi, J., Abbott, B. P., et al. 2015, CQGra, 32, 074001
LIGO/Virgo Scientific Collaboration, Abbott, B. P., Abbott, R., et al. 2016, ApJL, submitted (arXiv:1602.08492)
Loeb, A. 2016, ApJL, 819, L21
Lund, N., Budtz-Jørgensen, C., Westergaard, N. J., et al. 2003, A&A, 411, L231
Mereghetti, S., Götz, D., Borkowski, J., Walter, R., & Pedersen, H. 2003, A&A, 411, L291
Miller, J. C., Shahbaz, T., & Nolan, L. A. 1998, MNRAS, 294, L25
Moraes, P. H. R. S., & Miranda, O. D. 2014, MNRAS, 445, L11
Mösta, P., Palenzuela, C., Rezzolla, L., et al. 2010, PhRvD, 81, 064017
Palenzuela, C., Olabarrieta, I., Lehner, L., & Liebling, S. L. 2007, PhRvD, 75, 064005
Perna, R., Lazzati, D., & Giacomazzo, B. 2016, ApJL, submitted (arXiv:1602.05140)
Savchenko, V., Neronov, A., & Courvoisier, T. J.-L. 2012, A&A, 541, A122
Schunck, F. E., & Mielke, E. W. 2003, CQGra, 20, R301
Sturner, S. J., Shrader, C. R., Weidenspointner, G., et al. 2003, A&A, 411, L81
The LIGO Scientific Collaboration, & the Virgo Collaboration 2016, arXiv:1602.03840
Ubertini, P., Lebrun, F., di Cocco, G., et al. 2003, A&A, 411, L131
Vedrenne, G., Roques, J.-P., Schönfelder, V., et al. 2003, A&A, 411, L63
von Kienlin, A., Beckmann, V., Rau, A., et al. 2003, A&A, 411, L299
Winkler, C., Courvoisier, T. J.-L., di Cocco, G., et al. 2003, A&A, 411, L1
Woosley, S. E. 1993, ApJ, 405, 273
Zilhão, M., Cardoso, V., Herdeiro, C., Lehner, L., & Sperhake, U. 2012, PhRvD, 85, 124062